SAND99-0220C

Microseismic monitoring of the Mounds drill cuttings injection tests

N.R. Warpinski
Sandia National Laboratories
P.T. Branagan
Branagan & Associates
S.L. Wolhart
Gas Research Institute
Z.A. Moschovidis
Amoco Production Company
K.D. Mahrer
Branagan & Associates

ABSTRACT: This paper describes the microseismic mapping of repeated injections of drill cuttings into two separate formations at a test site near Mounds, OK. Injections were performed in sandstone and shale formations at depths of 830 and 595 m, respectively. Typical injection disposal was simulated using multiple small-volume injections over a three-day period, with long shut-in periods interspersed between the injections. Microseismic monitoring was achieved using a 5-level array of wireline-run, triaxial-accelerometer receivers in a monitor well 76 m from the disposal well. Results of the mapped microseismic locations showed that the disposal domain was generally aligned with the maximum horizontal stress with some variations in azimuth and that wide variations in height and length growth occurred with continued injections. These experiments show that the cuttings injection process can be adequately monitored from a downhole, wireline-run receiver array, thus providing process control and environmental assurance.

INTRODUCTION

Injection of slurries of ground drill cuttings into a deep formation is an environmentally attractive, cost-effective method for disposing of hydrocarbon-contaminated cuttings (Malachosky et al. 1993, Louviere & Reddoch 1993, Hainey et al. 1997, Bruno et al. 1995). However, the exact processes of fracturing, disaggregation, fracture branching, volumetric storage, and changes induced in the reservoir have not yet been fully identified (Abou-Sayed et al. 1989, Moschovidis et al. 1994, Wilson et al. 1993, Weng et al. 1997).

The Drill Cuttings Injection Experiment at a site near Mounds, OK, has the objectives of identifying the important mechanisms through a suite of monitored injections and the subsequent coring of the created fracture process zone. Monitoring techniques in this experiment include microseismic imaging, surface and downhole tiltmeter mapping, pressure monitoring and the application of various tracers, but this paper describes only the microseismic results.

The Mounds site layout is shown in Figure 1 and consists of a three-well pattern drilled to greater than 900-m depth. The injection well is in the center, while a microseismic monitor well is 76 m south of the injection well and a tiltmeter monitor well is 43 m north of the injection well. The known hydraulic fracture azimuth (Smith et al. 1985) is approximately east-west, so this layout provides a clear view of both wings of any induced fracture from either monitor well.

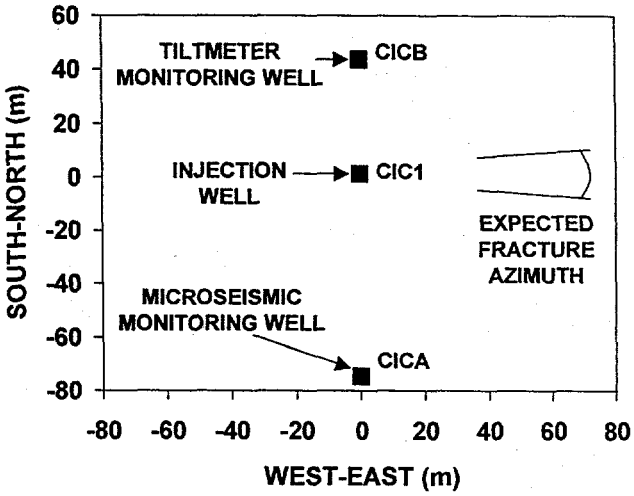

Figure 1. Mounds site layout.

As shown in Figure 2, injection experiments were conducted in two zones including an open-hole section of the Wilcox sandstone at a depth of approximately 830 m and at perforations from 591-597 m in the Atoka shale. In both zones, 5-level receiver arrays (Warpinski et al. 1998) were clamped across from the injection zone. These were

DISCLAIMER

then oriented using perforations and primer-cord shots in the treatment well and were left in place to monitor all of the injection tests. The spacing between individual receivers was 15.2 m.

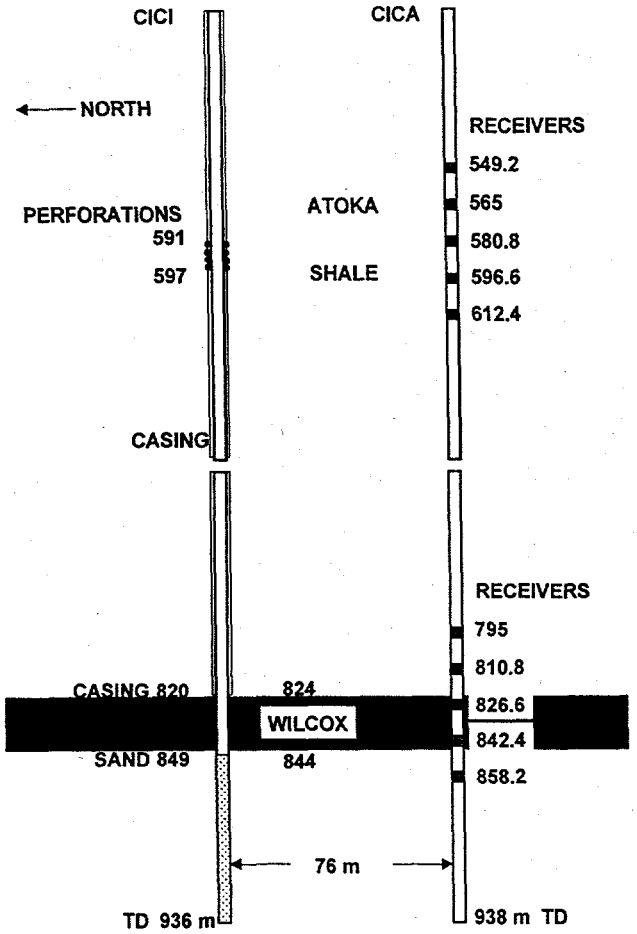

Figure 2. Side view of Wilcox and Atoka zones.

Injections in both zones consisted of a few water or drilling-mud injections for calibration testing, followed by repeated injections of 8 m^3 of ground and slurrified drill cuttings at concentrations of about 1.2 gm/cm^3. Long shut-in periods (relative to the pump time, ~ 2 hr) were interspersed between the injections. Testing in each zone concluded with somewhat larger injections (up to 16 m^3). A total of 17 cuttings injections were performed in the Wilcox sandstone and 20 cuttings injections were performed in the Atoka shale, each disposal zone having injections conducted over a three-day period. This testing occurred at the end of July, 1998.

MICROSEISMIC BACKGROUND

Microseismic monitoring has been proven to be a valuable technique for monitoring fractures induced by hydraulic fracturing in oil-field applications (Warpinski et al 1997), geothermal applications (Albright et al. 1982), and cuttings injection (Keck & Withers 1994). The changes in stress and pressure due to (1) the leakoff of high pressure liquids and (2) the dilation of a pressurized fracture are sufficient in many formations to generate shear slippage along pre-existing planes of weakness near the fracture. Such shear slippages emit seismic energy in a characteristic burst that can be detected with specialized receiver systems and analyzed for the source location. Tensile fractures may also occur, but these are less common, higher frequency, and more difficult to analyze. In weak zones, shear failure of the rock may occur, but it will likely emit less energy and be more difficult to detect. Thus, for microseismic monitoring to be effective, the shear slippages must be detected and located.

The rock slippage generates a significant shear (S) wave component of the microseism, while overriding of asperities or dropping into asperity voids provides the dilatational component that generates compressional (P) waves. For multiple receivers in a single well, only the P wave is absolutely required for source locations, but the addition of the S-wave information significantly increases the accuracy.

The horizontal distance to and elevation of the microseism can be calculated in many ways, particularly if the formation has relatively constant velocities and can be approximated as a homogeneous material. A fast method with an explicit solution is to perform a joint regression on the P-wave and S-wave arrival times to determine the three unknowns: distance, elevation, and origin time. Given a more complicated velocity structure, various advanced schemes are available. At the time of this paper, no final velocity structure information was available, so a uniform velocity was used for all of these calculations.

The final piece of information needed to locate the microseism is the azimuthal direction to the source from the monitor well. This parameter can be determined by using the knowledge that the particle motion of the P wave is parallel to the wave propagation direction, which in a uniform medium points directly back to the source. This directionality is determined by comparing the amplitudes of the two horizontal axes (often called a hodogram in graphical form) for the first 1-2 cycles of the P-wave motion. Although hodograms have a relatively large uncertainty in many cases, this is mitigated by obtaining azimuths on several receivers and using these statistics to improve the directional estimate.

Given the direction, horizontal distance and elevation, the microseism is fully located in three dimensional space. There is the final question of how the microseism is related to the fracture. Poro-mechanical analyses show that microseisms will be generated in a small region around the fracture tip where the stress concentration induces large shear

stresses, as well as any region that experiences significant increases in pore pressure due to the fluid leakoff (Warpinski 1994). Pore pressure increases reduce the net normal stress on planes of weakness (thus, reducing frictional forces) and allow them to slip under lower shear stresses than would be necessary in the virgin reservoir. Combining these two effects, it can be deduced that shear slippages are likely to be generated everywhere around the fracture and they may extend many meters normal to the fracture face if leakoff is large or the formation fluid compressibility is low. Thus, the microseismic locations form an envelope that surrounds the fracture providing general information about length, height, azimuth and asymmetry, but no information about width.

MOUNDS MICROSEISMS

Figure 3 shows an example microseism typical of those observed at this site. This figure displays grouped waveforms of the two horizontal axes (x,y) and the vertical axis (z) for all five levels, with the top data being the shallowest and the bottom being the deepest. Most microseisms here have P wave amplitudes (arriving at about 7-10 msec) that are much smaller than the S waves (arriving about 18-23 msec), but the P waves are still generally clear. The S waves are distinct on all levels except the center, probably because that receiver is in the null in the radiation pattern. Commonly, there is sufficient high frequency content to excite the 2200 Hz resonance of the accelerometers, giving the rather monofrequency appearance of the P waves on some levels. Dominant frequencies of both P and S waves are invariably greater than 1000 Hz.

During testing in the Wilcox sandstone, most injections induced about 15-50 detectable and analyzable microseisms, which is a significant number given the small size of the injections. The last Wilcox injection, a 16 m^3 test, induced nearly 80 microseisms. The Atoka injections were much less energetic, inducing only a few microseisms per injection. The reduced activity may be due to the lower stresses at the much shallower depth of the Atoka, or to characteristics of the formation, or both. As a result, however, it was impossible to image individual Atoka injections, although some information was provided on cumulative size and shape.

RESULTS OF MONITORING

The microseismic mapping results can be best displayed by showing both plan-view and side-view plots from separate injections and from the entire

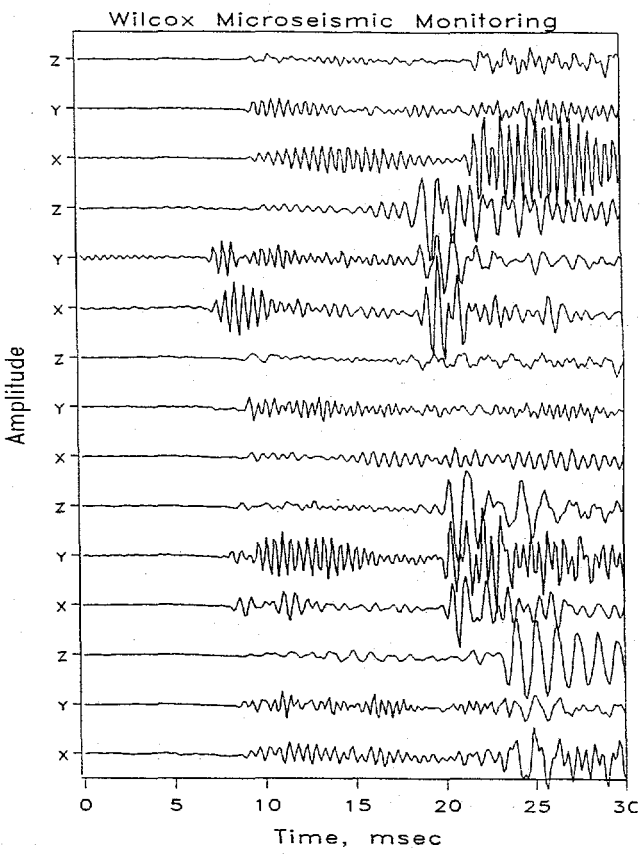

Figure 3. Example Wilcox microseism.

suite of injections, particularly for the Wilcox sandstone where there are many microseisms. Figure 4 shows the microseisms detected and located from the first cuttings injection into the Wilcox sandstone (8 m^3). The injection and monitor wells (rectangles) are plotted for reference in the plan-view plot, with the monitor well at (0,0). In the side view plot, the injection wellbore is represented by the vertical line, while the top and bottom of the Wilcox sandstone are represented by the horizontal lines. The side view of the microseisms shows their projection on a vertical plane having a strike given by the average azimuth of the microseisms as deduced from a linear regression. The diagnostic data in Figure 4 suggest that the fracture is highly asymmetric, growing primarily upward and to the east.

Uncertainties for these microseismic locations are shown in Figure 5. Error ellipsoids based on standard deviations of the regression and the azimuths are shown here in both views. The greatest error is associated with the azimuth to the microseism, due primarily to small amplitudes of the P waves. Even though the P waves are small relative to the noise, arrival times can often be accurately determined, but the hodograms have considerable uncertainty. The error ellipsoids in plan view are rotated perpendicular to the monitor well, which is the angular reference point. Finally, it can be seen that the sizable uncertainties do not

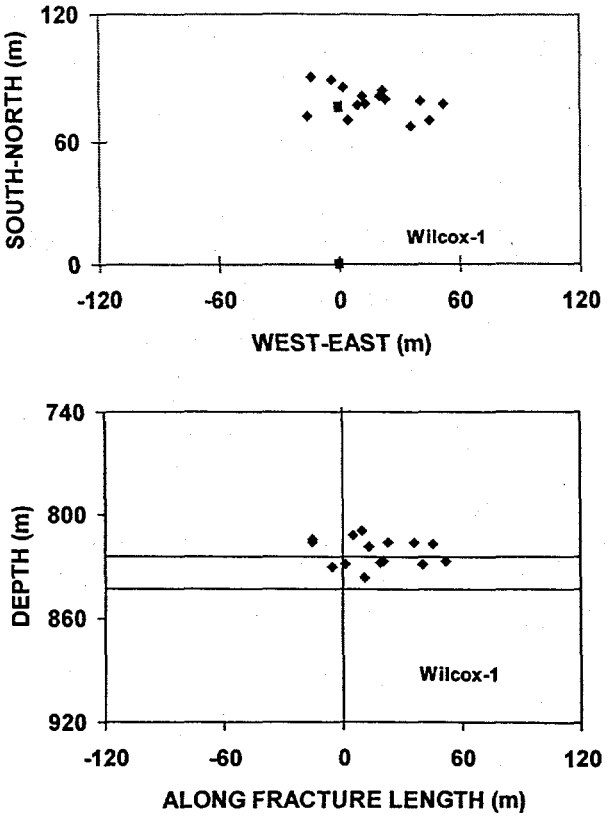

Figure 4. Plan-view and side-view maps of Wilcox injection #1.

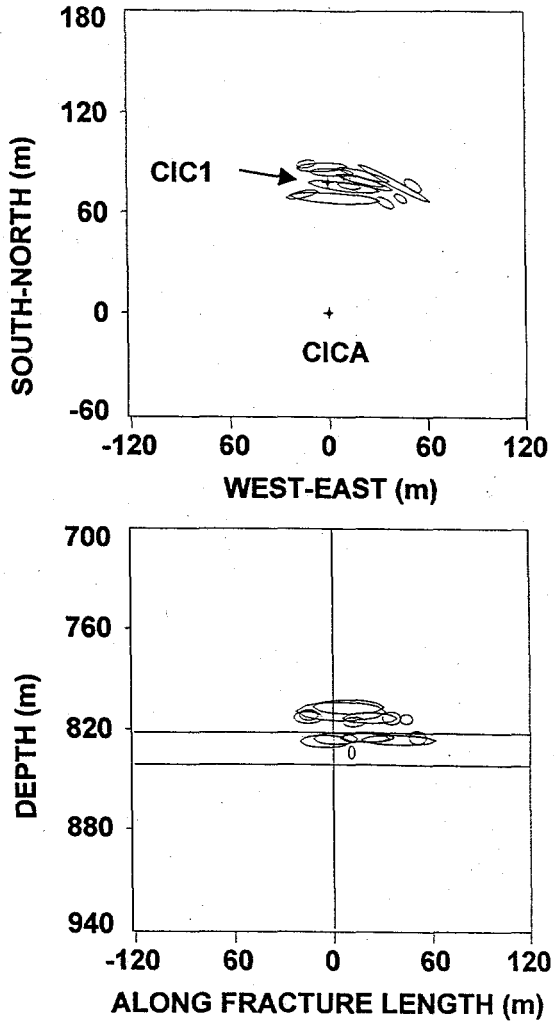

Figure 5. Uncertainty plots for Wilcox injection #1.

change interpretations of the data, so for this paper only the point maps (as in Figure 4) are shown.

The mapping results from the third microseismic injection are shown in Figure 6. By the third injection, the lateral asymmetry is considerably reduced, but there is mostly upward growth. This injection also appears to have more of a southeasterly trend than the injection #1, suggesting that it may have a different azimuth and possibly be a different fracture. Such a divergence in azimuths may occur due to plugging of the initial fracture with repeated injections, resulting in the disposal domain suggested by Moschovidis et al. (1994).

The pattern of nearly exclusive upward fracture growth continued during the first two days of testing. However, on the third day of testing, starting with injection #13, some downward microseismic activity also began to occur. Figure 7 shows the microseismic plots for this injection. It can be seen that the lateral growth is relatively symmetric and upward growth is still predominant, but some changes in stress, pressure or fracturing have triggered microseismic activity well below the Wilcox sandstone.

All of the microseismic activity observed in the Wilcox sandstone testing is shown in Figure 8. The plan-view plot shows a linear-trending cluster of microseisms having a primary axis just south of east, but with numerous outliers. From a single plot alone, it is impossible to distinguish whether this grouping is caused by a single hydraulic fracture or numerous fractures with orientations arrayed within the microseismic clusters. However, the additional data provided by the single-injection analyses suggest that some of the tests resulted in azimuths that appeared to be significantly different from the average (e.g., injection #3 shown in Figure 6). Thus, it is likely that the microseismic activity of Figure 8 is due to any number of fractures having azimuths ranging from about 85° to 125° (clockwise from N). The side view in Figure 8 shows a laterally symmetric fracture having mainly upward growth, with little activity in the Wilcox sandstone. It would appear that most of the material was injected near the casing shoe at 820 m into a fracture growing upward into the shales above the Wilcox. The activity below the Wilcox is perplexing, as it does not appear to be connected to the major fracturing events. The lower wellbore was a sand-filled open hole, so it is possible that injection materials channeled downhole and initiated a fracture at about 890 m. It is also possible that the lower microseismic activity is due to shear stresses

generated by the repeated injections and continued dilation of the fracture up above. However, the zone at 890 m would need to be very fragile to become active in response to fractures 80 m away. Possibly there is a permeable zone at this depth and liquids migrated into the zone, pressurizing it and causing the activity.

The Atoka fracturing results are shown in Figure 9. There are very few microseisms and most are small-amplitude events, so only the nearest events can be seen. This distribution of microseisms probably does not imply that the fracture is single winged, but more likely the microseisms on the west wing are too far from the monitor well to be resolved above the noise. The side-view plot shows that most of the activity is below the perforated interval (horizontal lines), with considerable downward growth.

DISCUSSION

These tests have shown that microseismic monitoring can be used to assess the injection of drill cuttings or other slurrified wastes in typical sedimentary formations. Even with the relatively small injections used in this demonstration, there were sufficient microseisms generated in the Wilcox testing to describe individual injections. The Atoka testing resulted in an order of magnitude fewer microseisms, but there were still sufficient numbers to provide an overall view of the fracture development. Given the larger injections typical of normal day-to-day disposal operations, much more energy would be available to induce increased numbers of larger microseisms.

The largest source of error in the microseismic locations was due to azimuthal uncertainty, primarily because the P-wave amplitudes were very low. The low amplitudes may be due to (1) the shear nature of the microseism (little P-wave energy generated), (2) to the monitor well being located in a null of the P-wave radiation pattern, or (3) attenuation of the high frequency P waves. However, since the natural fractures at this site strike NE and SE (Lorenz, pers. comm.), it is unlikely that the monitor well would not be favorably oriented for most of the activity. Thus, the probable reason for the small P waves is either source characteristics or transmission characteristics of the medium are unfavorable.

The small microseisms in the Atoka were not totally surprising, as a previous test at this site resulted in no observable microseismic activity in a sandstone at a depth of 320 m (Smith et al. 1985). The cause for the weak activity is probably small shear stresses at these shallow depths, although the shaley nature of the Atoka formation may contribute.

Table 1 shows the azimuths of the individual injections in the Wilcox formation and a day-by-day azimuth for the Atoka formation. The average azimuth is in good agreement with the 95° azimuth found by Smith (1985), but there are considerable variations about this value. Results of repeated injections using normal fracturing fluids has shown a scatter of only ±2-4° about the average azimuth (Warpinski et al., 1997), even for small calibration tests. The much large variations seen here suggest that there is a good possibility that new fractures are being induced at slightly different azimuths for some of the injections. This suggestion is borne out by the results of the coring through the fractures, where several fractures were found over zones encompassing most of these azimuths (Lorenz, pers. comm.) in both the Wilcox and the Atoka.

Table 1. Azimuths of Mounds injections.

Test	Injection #	Azimuth (deg)
Wilcox	1	97
	2	101
	3	107
	4	96
	5	96
	6	101
	7	97
	8	95
	9	99
	10	93
	11	86
	12	97
	13	97
	14	100
	15	98
	16	88
	17	96
	All	97
Atoka	Day 1	107
	Day 2	112
	Day 3	101
	All	106

The side view plots (e.g., Figures 4, 6 & 7) from the Wilcox tests indicate that individual injections result in microseismic activity that may proceed in considerably different directions from previous injections. Figure 10 shows contours (based on microseism locations) from selected injections that indicate the wide variety in growth behavior. Some of the tests resulted in entirely one-winged fractures, others had only activity above the Wilcox sandstone, and some were very symmetric. It appears that the each injection is creating new fractures or fingering through previously created fractures to generate the observed results.

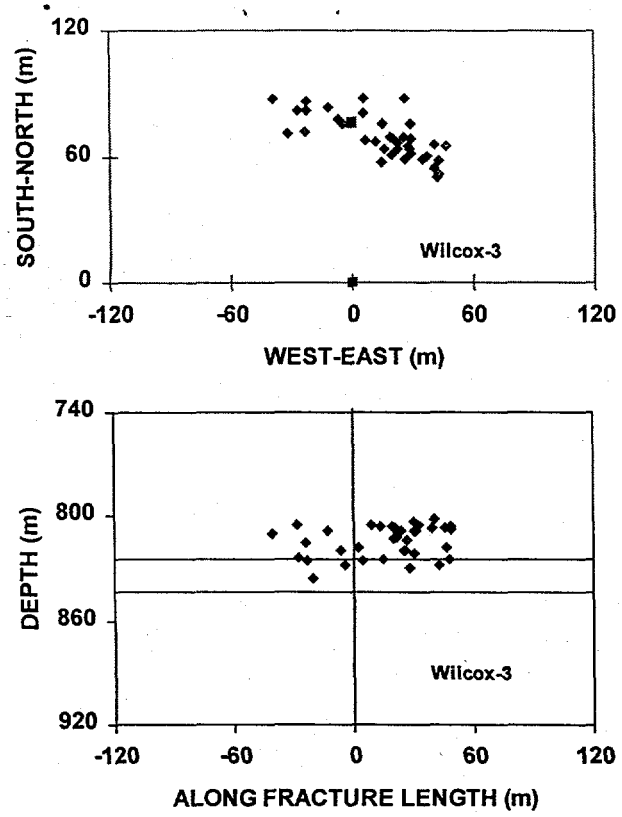

Figure 6. Microseismic activity associated with Wilcox injection #3.

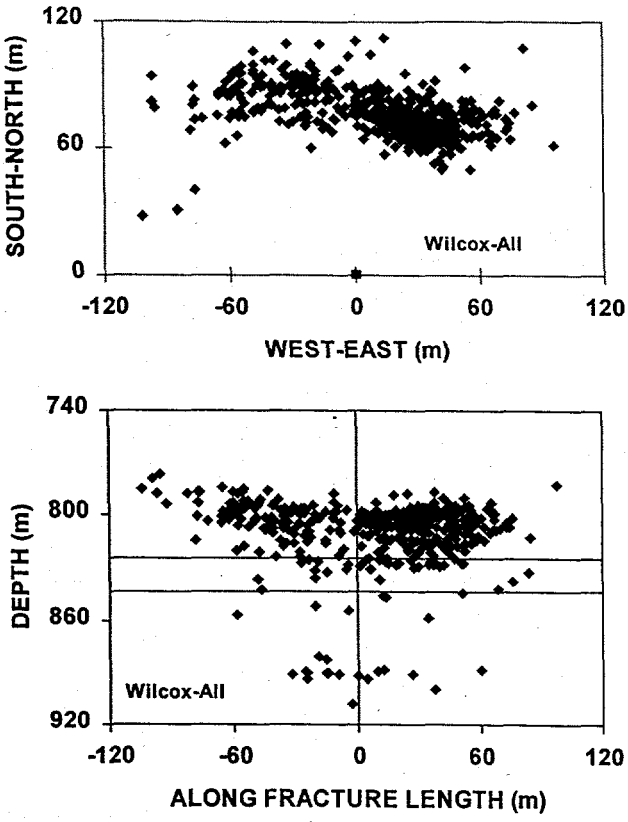

Figure 8. All Wilcox microseismic activity.

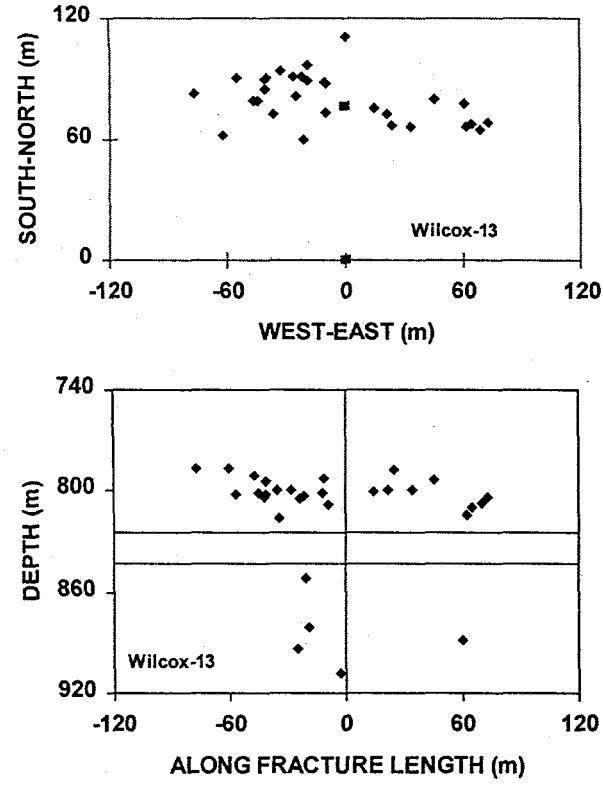

Figure 7. Microseismic activity associated with Wilcox injection #13.

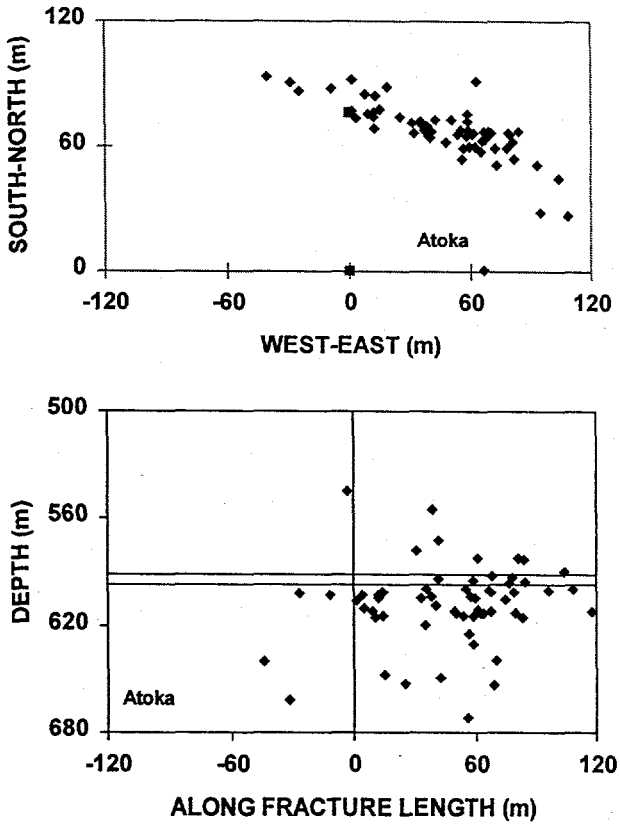

Figure 9. All Atoka microseismic activity.

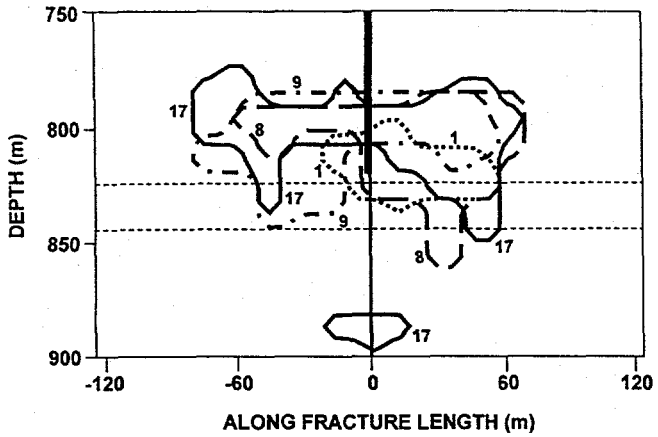

Figure 10. Fracture contours of selected Wilcox injections (numbers are the injection sequence).

Unfortunately, the geometries of the Atoka injections are not as clear as those in the Wilcox because of the small numbers of events. Although not shown in this paper, the activity from the first two days of pumping was confined to an approximately 50-m interval around the perforations. Most of the downward growth seen in Figure 9 occurred during the final day of injections.

It is also believed that the apparent lateral asymmetry is an artifact of the measurement process and not representative of the true dimensions. The microseisms in the Atoka were all extremely small and difficult to analyze. The additional distance that a microseism from the west wing would need to travel would in most cases make the P wave unidentifiable or analyzable for particle motion (hence, no azimuth could be obtained). Thus, there is no reason at this time to suspect that the fracture is not symmetric.

Many of the later Wilcox injections had "holes" of zero microseismic activity in the near-wellbore region in the vicinity of the casing shoe where the fracture most likely originated (e.g., Figure 7). We suggest that the reason for the lack of microseismic activity is that most of the near-wellbore slippage planes are activitated early in the injection process and unless some additional energy (higher pressure, new fracture plane, etc.) is provided, the already triggered slippage planes will not re-activate.

These results are based upon constant compressional and shear velocities in each interval. The average velocity was taken from the orientation shots in each interval, which provided numerous ray paths through the medium. When more detailed velocity information becomes available, these data will be re-located. It is not expected that the changes will be significant, but a carbonate just above the Wilcox sandstone is an extremely fast layer and may skew the height and distance somewhat. The most likely effect would be a slight change in azimuth. No changes are expected for the Atoka tests because the formation is very consistent throughout the zone of interest.

CONCLUSIONS

Microseismic monitoring of drill-cuttings injections was successfully performed in both sandstone and shale formations. Much more microseismic activity was observed in the Wilcox sandstone, but there was sufficient data in the Atoka shale to provide an overall view of the fracture geometry. The amount of microseismicity, given these small injections, is very encouraging for the monitoring of full-scale cuttings disposal.

Because of the small injections and shallow test depth, the microseism amplitudes (particularly the P waves) were very small, inducing larger uncertainty than normal. The largest uncertainty was in the azimuthal angle because of the difficulty in obtaining high-quality hodograms. However, the uncertainty had little effect on the interpretation of the data.

The results suggest that individual injections of the cuttings materials result in considerably different growth patterns and possibly azimuths. It is possible that new fractures are being created or the slurry materials are fingering through previous fractures, resulting in widely varying growth behavior.

Although not detailed in this paper, the microseismic results are in good agreement with downhole and surface tiltmeters and with cores taken through the fracture zone.

ACKNOWLEDGMENTS

The authors would like to thank the companies and the representatives of the Mounds Drill Cuttings Experiment Executive Committee for their funding and assistance. The companies include BP Exploration, Azerbaijan Oil Co., Schlumberger, Shell E&P Tech., Chevron, MSD, Halliburton Energy Services, Amoco, Mobil, Hughes-Christensen, Exxon Production Research, Arco, Gas Research Institute, Pinnacle Technologies and UPRC, as well as the US Dept. of Energy for its support under contract DE-FI04-91AL65092. Special thanks to the field support crew of Branagan & Associates, Rich Peterson for planning and management of many of the field activities, and Ed Chesney for his dedicated work at site management. The work at Sandia National Labs was performed for the Gas Research Institute.

REFERENCES

Abou-Sayed, A.S., D.E. Andrews & I.M. Buhidma 1989. Evaluation of oily waste injection below the permafrost in Prudhoe Bay field. SPE 18757, *Proc. SPE California Regional Mtg.*, Bakersfield CA: 129-142.

Albright, J.N. & C.F. Pearson 1982. Acoustic emissions as a tool for hydraulic fracture location. *SPE Journal* 22(4): 523-530.

Bruno, M.S., R.A. Bilak, M.B. Dusseault & L. Rothenburg 1995. Economic disposal of solid oil field wastes through slurry fracture injection. SPE 29646, *Proc. SPE Western Regional Mtg.*, Bakersfield, CA: 313-320.

Hainey, B.W., R.G. Keck, M.B. Smith, K.W. Lynch & J.W. Barth 1997. On-site fracturing disposal of oilfield waste solids in Wilmington field, Long Beach unit, CA. SPE 38255, *Proc. SPE Western Regional Mtg.*, Long Beach, CA: 77-84.

Keck, R.G. & R.J. Withers 1994. A field demonstration of hydraulic fracturing for solids waste injection with real-time passive seismic monitoring. SPE 28495, *Proc SPE Annual Tech. Conf. & Exh.*, New Orleans, LA: 319-334.

Louviere, R.J. & J.A. Reddoch 1993. Onsite disposal of rig-generated waste via slurrification and annular injection. SPE 25755, *Proc. SPE/IADC Drilling Conf.*, Amsterdam: 737-751.

Moschovidis, Z.A., D.C. Gardner, G.V. Sund & R.W. Veatch 1994. Disposal of oily cuttings by downhole periodic fracturing injections, Valhall, North Sea: case study and modeling concepts. SPE Drilling & Completion 9(4): 256-262.

Malachosky, E., B.E. Shannon, J.E. Jackson & W.G. Aubert 1993. Offshore disposal of oil-based drilling-fluid waste: an environmentally acceptable solution. *SPE Drilling & Completion* 8(4):283-287.

Smith, M.B., N.-K. Ren, G.G. Sorrells & L.W. Teufel 1985. A comprehensive fracture diagnostics experiment: part II – comparison of seven fracture azimuth measurements. SPE 13894, *Proc. SPE Low Permeability Gas Reservoirs Symp.*, Denver, CO: 443-458.

Warpinski, N.R. 1994. Interpretation of hydraulic fracture mapping experiments. SPE 27985, *Proc. Tulsa Centennial Petr. Eng. Symp.*, Tulsa, OK: 291-300.

Warpinski, N.R., P.T. Branagan, R.E. Peterson, J.E. Fix, J.E. Uhl, B.P. Engler & R. Wilmer 1997. Microseismic and deformation imaging of hydraulic fracture growth and geometry in the C sand interval, GRI/DOE M-Site project. SPE 38573, *Proc. SPE Annual Tech. Conf. & Exh.*, San Antonio, TX: 87-98.

Warpinski, N.R., P.T. Branagan, R.E. Peterson, S.L. Wolhart & J.E. Uhl 1998. Mapping hydraulic fracture growth and geometry using microseismic events detected by a wireline retrievable accelerometer array. SPE 40014, Proc. *SPE Gas Tech. Symp.*, Calgary, AB, Canada: 335-346.

Weng, X., A. Settaro & R.G. Keck 1997. A field demonstration of hydraulic fracturing for solids waste disposal – injection pressure analysis. *Int. J. Rock Mech. & Min. Sci.* 34:3-4, paper No. 331.

Wilson, S.M., M. Rylance & N.C. Last 1993. Fracture mechanics issues relating to cuttings re-injection at shallow depth. SPE 25756, *Proc. SPE/IADC Drilling Conf.* Amsterdam, 753-762.